Contribution from the Department of Chemistry,
University of Vermont, Burlington, Vermont 05405

Synthesis, Magnetic Susceptibility, and Mössbauer Spectra of Iron(III) Dimers and Iron(II) Polymers Containing 2,5-Dihydroxy-1,4-benzoquinones

JAMES T. WROBLESKI and DAVID B. BROWN*

Received May 31, 1978

Several iron complexes of the dianions of 2,5-dihydroxy-1,4-benzoquinone (DHBQ) and 2,5-dichloro-3,6-dihydroxy-1,4-benzoquinone (CA, chloranilate dianion) have been prepared and studied by magnetic susceptibility and Mössbauer spectroscopic methods. Iron(II) salts react with these dihydroxybenzoquinones to give polymeric $Fe(DHBQ)(H_2O)_2$ and $Fe(CA)(H_2O)_2$. If the reaction is carried out in the presence of pyrazine, pyr, $[Fe(CA)(pyr)]_n$ and $[Fe(DHBQ)(pyr)]_n$ are obtained. Infrared spectral results are consistent with the presence of bridging bidentate pyr in these complexes and thus sheet polymers. Dimeric $Fe_2(DHBQ)_3(H_2O)_4$ and $Fe_2(CA)_3(H_2O)_4 \cdot 4H_2O$ are obtained by reacting $FeCl_3$ with the respective dihydroxybenzoquinone. Magnetic susceptibility vs. temperature data obtained for the polymeric materials are fit to an $S = 2$ Heisenberg linear-chain model with $J \simeq -1.4$ cm^{-1} for $[Fe(DHBQ)(H_2O)_2]_n$ and $J \simeq -2.6$ cm^{-1} for $[Fe(DHBQ)(pyr)]_n$. Corresponding values for the CA-containing polymers are $J > -0.1$ cm^{-1} and $J \simeq -0.5$ cm^{-1}, respectively. The Heisenberg–Dirac–Van Vleck $S_1 = S_2 = {}^5/_2$ spin exchange model applied to the magnetic susceptibility vs. temperature data for $Fe_2(DHBQ)_3(H_2O)_4$ and $Fe_2(CA)_3(H_2O)_4 \cdot 4H_2O$ yields $J = -2.0$ cm^{-1} and $J = -1.0$ cm^{-1}, respectively. The presence of an anisotropy in the recoilless fraction (Goldanskii–Karyagin effect) is observed in the ^{57}Fe Mössbauer spectra of the Fe(III) dimers and is substantiated by measurements on the temperature dependence of the Mössbauer parameters.

Introduction

Several recent investigations have established that dianions of 2,5-dihydroxy-1,4-benzoquinones (I) are capable of bridging

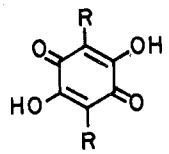

Ia, R = H (dihydroxybenzoquinone, $DHBQH_2$)
Ib, R = Cl (chloranilic acid, CAH_2)

transition-metal ions to form dimers and coordination polymers. For example, 1:1 coordination polymers of the dianion of Ib with Co(II),[1-3] Ni(II),[1,2,4-7] Cu(II),[1,2,7,8] Sn(IV),[9] Pt(II),[10] and Pd(II)[10] were prepared and, in some instances, their optical and magnetic properties measured. Pierpont et al.[11] recently reported the structures and magnetic exchange parameters for several Ni(II) and Cu(II) dimers containing bridging dianions of Ia and Ib with terminal 2,2′,2″-triaminotriethylamine, 1,1,4,7,7-pentamethyldiethylenetriamine, and dipropylenetriamine ligands. In addition, a report of the X-ray structure of a Pd dimer, $K_2[PdClL]_2$ (L = Ib), has also appeared.[12]

In this paper we report syntheses and characterization of polymeric Fe(II) and dimeric Fe(III) complexes of dianions of these dihydroxybenzoquinones. Prior to this work no iron chelates of Ia or Ib had been well characterized. However, Beg[10] prepared an Fe(III) complex of the dianion of Ib for which he proposed a polymeric structure, principally on the basis of analytical and IR data. In apparent contradiction to both that report and this work, Cabbiness and Amis[4] reported the formation of a bis Fe(III) complex of Ib in aqueous solution. Our original purpose in undertaking this study was primarily to compare the magnitude of magnetic exchange in iron complexes of I with that in iron complexes of similar oxygen-donor ligands. We also sought to compare the magnetic exchange exhibited by these compounds to those previously reported for polymers and dimers containing bridging dianions of I.[3,8,11] During the course of this investigation we also observed interesting Mössbauer spectral behavior for the dimeric compounds. Results of variable-temperature, zero-field Mössbauer experiments are included in this paper.

Experimental Section

Both CAH_2 and $DHBQH_2$ were purchased from Eastman Chemical Co. and were purified either by recrystallization from ethanol or by vacuum sublimation.[13] All other compounds used in the syntheses were reagent grade materials and were used as received from the supplier.

Preparation of Complexes. $[Fe(CA)(H_2O)_2]_n$. Polymeric diaquochloranilatoiron(II) was prepared under an atmosphere of N_2 by slowly adding a degassed aqueous solution of $FeSO_4 \cdot 7H_2O$ (1.14 g, 4.05 mmol) to a hot aqueous solution of CAH_2 (0.85 g, 4.05 mmol). The resulting solution was stirred at reflux for 15 min and then quickly cooled to room temperature and filtered. The dark green precipitate was washed with water and then ethanol and finally dried in vacuo at 100 °C. Anal. Calcd for $C_6Cl_2FeH_4O_6$: C, 24.11; Cl, 23.73; Fe, 18.69; H, 1.35. Found: C, 23.98; Cl, 23.86; Fe, 18.8; H, 1.22.

$[Fe(DHBQ)(H_2O)_2]_n$. Polymeric diaquodihydroxybenzoquinonatoiron(II) was prepared and isolated in a similar manner to that of $[Fe(CA)(H_2O)_2]_n$. Anal. Calcd for $C_6FeH_6O_6$: C, 31.34; Fe, 24.29; H, 2.63. Found: C, 31.38; Fe, 24.3; H, 2.44.

$[Fe(CA)(pyr)]_n$. A pyrazine analogue of $[Fe(CA)(H_2O)_2]_n$ was prepared by adding solid $FeSO_4 \cdot 7H_2O$ (5.64 g, 20.3 mmol) to a refluxing methanol solution (250 mL) containing pyrazine (1.63 g, 20.3 mmol). The red-orange iron(II)–pyrazine complex which precipitated was redissolved by adding 25 mL of water to this mixture. A concentrated aqueous solution of CAH_2 (4.24 g, 20.3 mmol) was added giving a brown-black precipitate. This precipitate was washed with 500 mL of hot water and then with 250 mL of ethanol, and finally it was air-dried at room temperature over P_2O_5. Anal. Calcd for $C_{10}Cl_2FeH_4N_2O_4$: C, 35.03; H, 1.18; N, 8.17. Found: C, 34.82; H, 1.02; N, 7.69.

$[Fe(DHBQ)(pyr)]_n$. This pyrazine complex was prepared in a manner exactly analogous to that of $[Fe(CA)(pyr)]_n$. The brown-black precipitate was dried in vacuo at room temperature over $CaSO_4$. Anal. Calcd for $C_{10}FeH_6N_2O_4$: C, 43.83; Fe, 20.38; H, 2.21; N, 10.22. Found: C, 43.49; Fe, 20.4; H, 2.21; N, 10.62.

$Fe_2(CA)_3(H_2O)_4 \cdot 4H_2O$. Tetraaquotrichloranilatodiiron(III) tetrahydrate was prepared by adding stoichiometric amounts of $FeCl_3 \cdot 6H_2O$ and CAH_2 to a stirred solution of ethanol containing 10% water by weight. A dark black precipitate formed immediately. This precipitate was repeatedly washed with hot ethanol and twice recrystallized from hot water to yield a blue-black microcrystalline product. Anal. Calcd for $C_{18}Cl_6Fe_2H_{16}O_{20}$: C, 24.66; Cl, 24.26; Fe, 12.74; H, 1.84. Found: C, 24.71; Cl, 23.58; Fe, 12.6; H, 1.59.

$Fe_2(DHBQ)_3(H_2O)_4$. Tetraaquotris(dihydroxybenzoquinonato)diiron(III) was prepared in a similar manner to that of $Fe_2(CA)_3(H_2O)_4 \cdot 4H_2O$ except that anhydrous $FeCl_3$ was used instead of $FeCl_3 \cdot 6H_2O$. The recrystallized product was a dark brown microcrystalline material. Anal. Calcd for $C_{18}Fe_2H_{14}O_{16}$: C, 36.15; Fe, 18.68; H, 2.36. Found: C, 35.84; Fe, 18.4; H, 2.23.

Physical Measurements. Magnetic susceptibilities were determined on polycrystalline samples by using a conventional Faraday balance[14] calibrated with $Hg[Co(NCS)_4]$.[15] Corrections for ligand diamagnetism were calculated from a table of Pascal's constants.[16] Experimental magnetic susceptibilities and moments were fit to theoretical ex-

0020-1669/79/1318-0498$01.00/0 © 1979 American Chemical Society

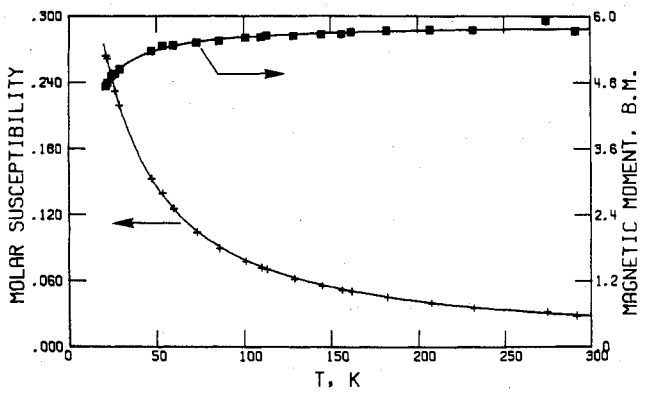

Figure 1. Corrected molar paramagnetic susceptibility ($\bar{\chi}_M$, cgsu) and effective magnetic moment per iron ($\bar{\mu}_{eff}$, μ_B) vs. temperature for $Fe_2(CA)_3(H_2O)_4 \cdot 4H_2O$. The solid curve is a fit to the HDVV $S_1 = S_2 = {}^5/_2$ dimer model with $J = -0.95$ cm^{-1}, $g = 2.00$, and $N\alpha = 0.0$.

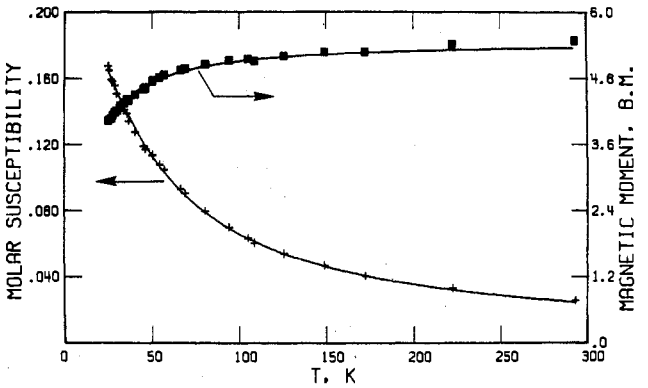

Figure 2. Corrected molar paramagnetic susceptibility ($\bar{\chi}_M$, cgsu) and effective magnetic moment per iron ($\bar{\mu}_{eff}$, μ_B) vs. temperature for $Fe_2(DHBQ)_3(H_2O)_4$. The solid curve is a fit to the HDVV $S_1 = S_2 = {}^5/_2$ dimer model with $J = -2.00$ cm^{-1}, $g = 2.00$, and $N\alpha = 0.0$.

pressions with a local computer routine which employs the Simplex minimization algorithm.[17] A number of goodness-of-fit criteria, including the standard error of estimate (standard deviation)[18] and the χ^2 test (eq 1), were applied to fits obtained in this manner.

$$\chi^2 = \sum_{i=1}^{n} \{[\bar{\chi}_M(\text{obsd})_i - \bar{\chi}_M(\text{calcd})_i]^2 / \bar{\chi}_M(\text{calcd})_i\} / (n-k) \quad (1)$$

Mössbauer spectra were obtained on a spectrometer previously described.[19] The source was ^{57}Co(Pd) which was maintained at room temperature in all cases. A 25-μm α-Fe foil (430 μg of ^{57}Fe/cm^2) was used as a velocity scale calibrant. Mössbauer spectra were deconvoluted by assuming Lorentzian line contours superimposed on a parabolic baseline. Standard error propagation equations which require the variance in the parameters of best fit were employed to ascertain the error limits on the final Mössbauer parameters.[20] Mössbauer spectra were taken in all cases on finely ground polycrystalline samples dispersed in Vaseline and held in a lead block between Fe-free Mylar tape.

Infrared spectra were obtained on a Beckman IR 20A with KBr pressed pellets. TGA curves were taken on a Du Pont 900 thermal analyzer coupled to a Du Pont 950 thermogravimetric analyzer. Iron was determined by EDTA titrimetry.[21] C, H, N, and Cl determinations were performed by Integral Microanalytical Laboratories, Inc., Raleigh, N.C.

Results and Discussion

The following abbreviations are used in this section: DHBQ is the dianion of 2,5-dihydroxy-1,4-benzoquinone (Ia), CA is the dianion of 3,6-dichloro-2,5-dihydroxy-1,4-benzoquinone (Ib, chloranilate dianion), and pyr refers to the neutral pyrazine ligand. The six complexes prepared above are stable for long periods of time if stored over $CaSO_4$. Although $Fe_2(DHBQ)_3(H_2O)_4$ and $Fe_2(CA)_3(H_2O)_4 \cdot 4H_2O$ are slightly soluble in water, Me_2SO, and CH_3CN, we were unable to obtain useful molecular weight data for these compounds. The remaining four complexes are characterized by their marked insolubility in all solvents tested. This insolubility supports a polymeric structure for these materials. Replicate preparations of these polymers resulted in analytically and magnetically indistinguishable materials. Several attempts were made to synthesize the pyridine adducts of $[Fe(CA)(H_2O)_2]_n$ and $[Fe(DHBQ)(H_2O)_2]_n$. Compounds obtained in such cases were very unstable and were characterized by rapid loss of pyridine with concomitant metal oxidation.

Magnetic Susceptibility of the Dimers. The magnetic susceptibility behavior of $Fe_2(CA)_3(H_2O)_4 \cdot 4H_2O$ and $Fe_2(DHBQ)_3(H_2O)_4$ over the temperature range 20–300 K is characteristic of that expected for antiferromagnetic spin exchange. Figures 1 and 2 show a monotonic decrease in $\bar{\mu}_{eff}$ for $Fe_2(CA)_3(H_2O)_4 \cdot 4H_2O$ and $Fe_2(DHBQ)_3(H_2O)_4$, respectively. The $\bar{\mu}_{eff}$ value for $Fe_2(CA)_3(H_2O)_4 \cdot 4H_2O$ drops from 5.81 μ_B at 290 K to 4.74 μ_B at 21 K. Similarily for $Fe_2(DHBQ)_3(H_2O)_4$, $\bar{\mu}_{eff}$ falls from 5.55 μ_B at 290 K to 4.04 μ_B at 24 K. A complete listing of experimental and calculated susceptibility data is given in Table I.[22] Susceptibility data for these two compounds were fit to expression 2 which is the

$$\bar{\chi}_M = (2N\beta^2g^2/kT)[55 + 30\exp(-10J/kT) + 14\exp(-18J/kT) + 5\exp(-24J/kT) + \exp(-28J/kT)]/[11 + 9\exp(-10J/kT) + 7\exp(-18J/kT) + 5\exp(-24J/kT) + 3\exp(-28J/kT) + \exp(-30J/kT)] + N\alpha \quad (2)$$

appropriate equation for an $S_1 = S_2 = {}^5/_2$ Heisenberg–Dirac–Van Vleck dimer model ($H = -2J\hat{S}_1 \cdot \hat{S}_2$). To obtain the fits shown in Figures 1 and 2 only the isotropic exchange parameter J was varied. Both g and $N\alpha$ were held constant at 2.00 and 0.0, respectively. These values are appropriate for an ion with a $^6A_{1g}$ ground term.[23] Best fit values of J for $Fe_2(CA)_3(H_2O)_4 \cdot 4H_2O$ and $Fe_2(DHBQ)_3(H_2O)_4$ are -1.0 and -2.0 cm^{-1}, respectively. These values are similar to those obtained by Pierpont et al.[11] for DHBQ- and CA-bridged Ni(II) and Cu(II) dimers (range -1.1 to -4.6 cm^{-1}). Dimeric structure II is consistent with these small values of J. This

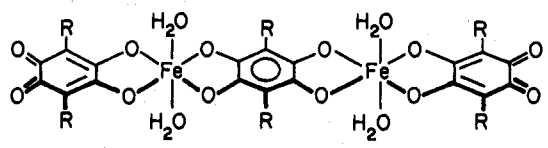

II

structure is unique in that both bridging and terminal dihydroxybenzoquinone ligands are present. We assume a planar structure for the central core containing the iron ions and the bridging ligand. Such a situation is consistent with structural information obtained by Pierpont et al.[11] for DHBQ- and CA-bridged Ni(II) and Cu(II) dimers. As discussed later, infrared arguments are consistent with chelated rather than monodentate CA and DHBQ ligands. The infrared spectra of these dimers are also consistent with the presence of both bridging and terminal quinone ligands.

Unlike the copper(II) complexes,[11] the Fe(III) ground state is relatively insensitive to changes in the ligand field. This is illustrated by comparing the magnitude of the exchange parameter in several oxygen-donor Fe(III) dimers. Some typical data are presented in Table II. Although quantitative arguments regarding J are difficult to substantiate from these data, it is clear that an increase in the number of bridging atoms increases the barrier to spin exchange in these Fe(III) dimers. By contrast, the magnitude of spin exchange in a series of copper(II) dimers containing oxalate, squarate, and dihydroxybenzoquinone bridges appears to depend more upon the coordination about the copper (and hence the electronic structure of the copper(II) ion) than upon the nature of the

Table II. Magnetic Exchange Parameters for Fe(III) Dimers with Various Oxygen Bridging Units[a]

compd	bridging unit	no. of bridging units per dimer	J, cm^{-1}	ref
$Fe_2(CA)_3(H_2O)_4 \cdot 4H_2O$	$C_6Cl_2O_4$	1	−0.95	this work
$Fe_2(DHBQ)_3(H_2O)_4$	$C_6H_2O_4$	1	−2.00	this work
$[Fe_2(sq)(phen)_4]Cl_4$	C_4O_4	1	−3.2	24
$[Fe_2(ox)(phen)_4]Cl_4$	C_2O_4	1	−6.8	24
$[Fe(sq)(OH)(H_2O)_2]_2 \cdot 2H_2O$	OH	2	−6.9	25
$[Fe(dipic)(OH)(H_2O)]_2$	OH	2	−11.4	26
$\{[Fe(bpy)_2]_2O\}Cl_4$	O	1	−105	27, 28

[a] Abbreviations: sq = squarate dianion, phen = 1,10-phenanthroline, dipic = 2,6-pyridinedicarboxylate, bpy = 2,2′-bipyridine.

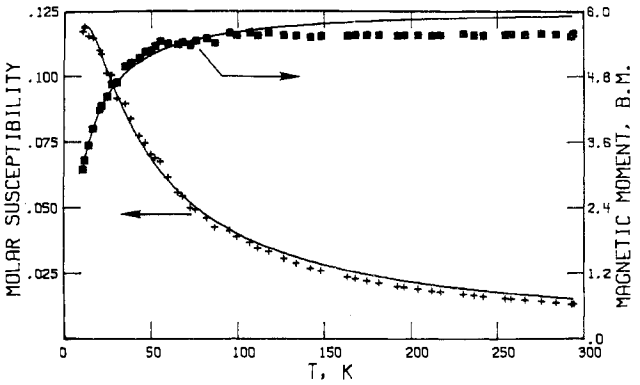

Figure 3. Corrected molar paramagnetic susceptibility ($\bar{\chi}_M$, cgsu) and effective magnetic moment per iron ($\bar{\mu}_{eff}$, μ_B) vs. temperature for $[Fe(DHBQ)(H_2O)_2]_n$. The solid curve is a fit to the $S = 2$ Heisenberg linear-chain model with $J = -1.35$ cm^{-1}, $g = 2.14$, and $N\alpha = 55 \times 10^{-6}$ cgsu.

bridging ligand.[11,29] In a series of nickel(II) complexes with these same bridging ligands, it was observed[11] that exchange was smaller with the squarate bridge than with the more extended dihydroxybenzoquinone bridge. This rather surprising result was rationalized in terms of the energies of the available orbitals on the bridging ligands. Our results (Table II) give the reverse order for the magnitude of exchange through these two ligand bridges. In *both* the Ni(II) and Fe(III) cases, however, the change in ligand bridge is also accompanied by changes in the other ligands. Unless a series of materials can be prepared in which all other factors remain constant, caution should be exhibited in attempting to explain what are relatively small differences in the magnitude of exchange parameters.

Magnetic Susceptibility of the Polymers. Corrected molar susceptibility and effective magnetic moment curves for polymeric $Fe(DHBQ)(H_2O)_2$ are shown in Figure 3. Experimental and calculated susceptibilities and magnetic moments are given in Table I.[22] The value of $\bar{\mu}_{eff}$ is essentially unchanged from 5.6 μ_B in the temperature range 60–300 K. Below 60 K $\bar{\mu}_{eff}$ falls monotonically reaching 3.10 μ_B at 10 K. It appears that although an antiferromagnetic exchange mechanism dominates the susceptibility behavior at $T \lesssim 100$ K, some additional mechanism must be adopted to explain the susceptibility at $T > 100$ K. Although the data points shown in Figure 3 result from a single experiment on one preparation, replicate runs using three different sample preparations gave identical (±0.03 μ_B) results. These data were fit to several theoretical magnetic susceptibility models in order to propose a structural model for this compound. The axially symmetric spin–orbit coupling matrix elements of Figgis et al.[30] were used in tabular form[31] to approximate the $\bar{\mu}_{eff}$ vs. T curve in terms of the orbital reduction parameter **k**. The term spin–orbit coupling constant was held constant at −100 cm^{-1}. Although the high-temperature data ($|kT/\lambda| > 0.3$) were fit within experimental error to the parameters **k** = 1.0 and $\nu = -1$, no suitable fit was found for $|kT/\lambda| \lesssim 0.3$. Both the Heisenberg[32] and Ising[33] linear-chain models were used in fitting the data. Equation 3 is the classical expression[32] (with inclusion of a

$$\bar{\chi} = \frac{2N\beta^2g^2}{kT}\left(\frac{1 + \coth(x - 1/x)}{1 - \coth(x + 1/x)}\right) + N\alpha \qquad (3)$$

temperature-independent term, $N\alpha$) for a Heisenberg chain of $S = 2$ ions, where $x = 12J/kT$. Whereas application of the Ising model yielded chemically unreasonable fits,[34] the Heisenberg model was found to provide a reasonable description of the data, particularly in the $T < 100$ K region. The fit obtained for $J = -1.4$ cm^{-1}, $g = 2.14$, and $N\alpha = 55 \times 10^{-6}$ cgsu is shown as the solid curve in Figure 3. Application of the Heisenberg linear-chain model to the data for $[Fe(CA)(H_2O)_2]_n$ (Table I)[22] gave a very good fit for $J \approx -0.1$ cm^{-1}, $g = 2.14$, and $N\alpha = 55 \times 10^{-6}$ cgsu. The character of this fit for $[Fe(CA)(H_2O)_2]_n$ is not very instructive because of the very small temperature dependence of $\bar{\mu}_{eff}$ (5.8 μ_B at 300 K to 5.5 μ_B at 20 K). The value of J for $[Fe(DHBQ)(H_2O)]_n$ is considerably smaller than that observed by Kobayashi et al.[8] for polymeric Cu(DHBQ). These workers found sample-dependent values of J in the range −9.7 to −16.7 cm^{-1}. In the absence of a single-crystal structure for these polymers it is difficult to attach quantitative significance to these values of the exchange parameter. In addition, we have not satisfactorily accounted for the susceptibility behavior at $T > 100$ K in $[Fe(DHBQ)(H_2O)_2]_n$. Although a number of situations, including variable chain length polymers and rings, may be invoked for an explanation, experimental evidence does not support these models in this case. An interesting possibility will be discussed later in connection with the Mössbauer spectra of these compounds. There is the possibility that chain-terminating iron(III)–quinone units would account for the susceptibility at high temperatures. Such a situation would result in a lower J but the result is not quantitatively available. Thus the magnetic data for $[Fe(DHBQ)(H_2O)_2]_n$ and $[Fe(CA)(H_2O)_2]_n$ do not allow us to distinguish the two possible polymeric structures III and IV from one another. We have

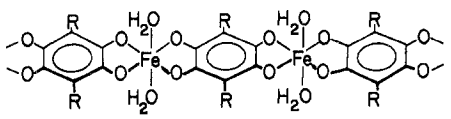

III

eliminated the coordinated water molecules from structure IV for purposes of clarity. Structure III is favored on intuitive grounds and by analogy to reported structures[11] of other metal complexes of dihydroxybenzoquinones. Structure IV, however, is similar to that found for nickel(II) squarate dihydrate,[35] and this structure cannot be ruled out on the basis of our data.

Corrected molar susceptibilities and effective magnetic moments for $[Fe(DHBQ)(pyr)]_n$ and $[Fe(CA)(pyr)]_n$ are illustrated in Figures 4 and 5, respectively. Experimental and calculated susceptibilities and magnetic moments are included

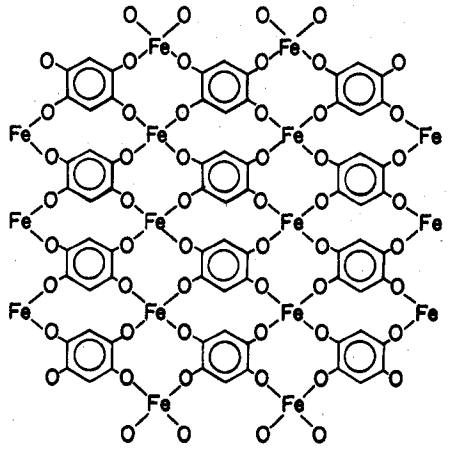

IV

in Table I.[22] These two compounds show somewhat greater antiferromagnetic exchange relative to their aquo analogues. The value of $\bar{\mu}_{eff}$ for $[Fe(DHBQ)(pyr)]_n$ drops from 5.0 μ_B at 298 K to 2.1 μ_B at 12 K. The value of $\bar{\mu}_{eff}$ for $[Fe(CA)(pyr)]_n$ decreases at a slower rate from 5.2 μ_B at 214 K to 4.2 μ_B at 14 K. As shown in Figures 4 and 5, good fits were obtained by using the Heisenberg linear-chain model. The solid curve shown in Figure 4 is obtained for $J = -2.6$ cm^{-1}, $g = 2.14$, and $N\alpha = 55 \times 10^{-6}$ cgsu. Similarily for $[Fe(CA)(pyr)]_n$ (Figure 5), $J = -0.5$ cm^{-1}, $g = 2.14$, and $N\alpha = 25 \times 10^{-6}$ cgsu. A maximum in the susceptibility vs. temperature curve near 20 K is clearly visible in Figure 4 for the DHBQ compound. As before, replicate data sets showing insignificant differences between them were obtained for these polymers.

Pyrazine is known to act as an effective bridging ligand in several polymeric materials, notably, $[Cu(pyr)_2(NO_3)_2]_n$,[36] $[(bpy)_2ClRu(pyr)[Ru(bpy)_2(pyr)]_nRuCl(bpy)_2](PF_6)_{2n+2}\cdot(n + 2)H_2O$,[37] and $[CoCl_2(pyr)]_n$.[38] The first two compounds are linear chains containing bridging pyrazine molecules while the Co(II) complex is a two-dimensional sheet polymer also containing bridging pyrazines. Single-crystal susceptibility data for $[Cu(pyr)_2(NO_3)_2]_n$ were analyzed in terms of the Heisenberg model.[39] The value of J was given[39] as -3.7 cm^{-1}. A possible structure for $[Fe(quinone)(pyr)]_n$ containing bridging pyrazine is shown as structure V. It is perhaps

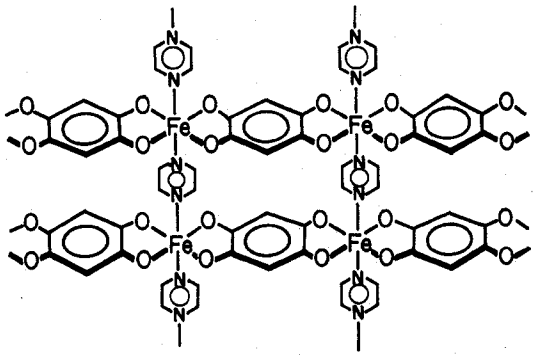

V

surprising that this structure would exhibit susceptibility vs. temperature behavior so characteristic of a linear-chain material, although such behavior would be expected if pyrazine provides a more facile pathway for exchange than the dihydroxybenzoquinone ligands.

Mössbauer Spectra of the Polymers. The room-temperature spectrum of $[Fe(CA)(H_2O)_2]_n$, shown in Figure 6, consists of a single quadrupole doublet with $\delta = 1.16$ mm/s and $\Delta E_Q = 2.50$ mm/s.[40] A complete listing of Mössbauer spectral parameters for the six quinone complexes discussed in this report is given in Table III.[22] We observe a slight increase

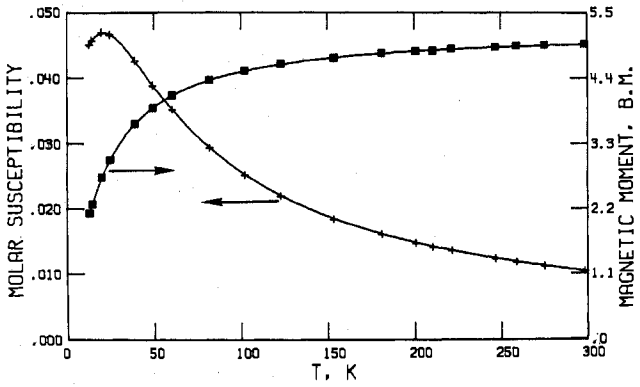

Figure 4. Corrected molar paramagnetic susceptibility ($\bar{\chi}_M$, cgsu) and effective magnetic moment per iron ($\bar{\mu}_{eff}$, μ_B) vs. temperature for $[Fe(DHBQ)(pyr)]_n$. The solid curve is a fit to the $S = 2$ Heisenberg linear-chain model with $J = -2.55$ cm^{-1}, $g = 2.14$, and $N\alpha = 55 \times 10^{-6}$ cgsu.

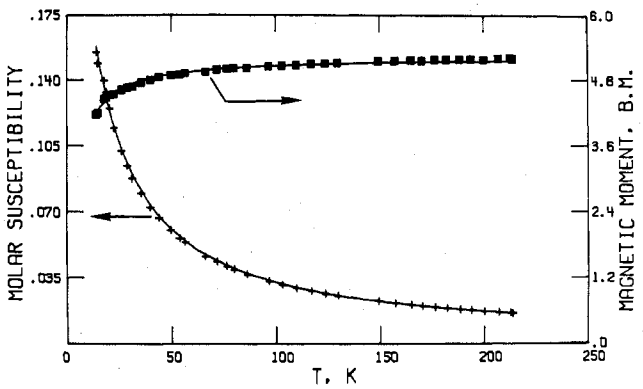

Figure 5. Corrected molar paramagnetic susceptibility ($\bar{\chi}_M$, cgsu) and effective magnetic moment per iron ($\bar{\mu}_{eff}$, μ_B) vs. temperature for $[Fe(CA)(pyr)]_n$. The solid curve is a fit to the $S = 2$ Heisenberg linear-chain model with $J = -0.54$ cm^{-1}, $g = 2.14$, and $N\alpha = 25 \times 10^{-6}$ cgsu.

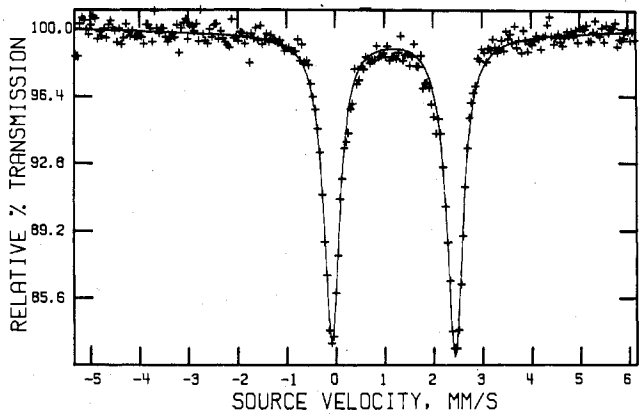

Figure 6. Room-temperature Mössbauer spectrum of $[Fe(CA)(H_2O)_2]_n$. The solid curve is a fit to the parameters given in Table III[22] (8 mg of Fe/cm^2).

in both ΔE_Q and δ with decreasing temperature. Thus, at 15 K $\delta = 1.21$ mm/s and $\Delta E_Q = 2.69$ mm/s. Such small increases in these parameters (ca. 10–20%) are attributable to a second-order Doppler effect.[41] The room-temperature spectrum of $[Fe(DHBQ)(H_2O)_2]_n$, shown in Figure 7, consists of two quadrupole doublets. This spectrum was fit to four lines by constraining the two most intense lines (assigned to the divalent iron site) to be identical. The result of this fit gives the following parameters (see Table III[22]): Fe(II) site, $\delta = 1.16$ and $\Delta E_Q = 1.47$ mm/s; Fe(III) site, $\delta = 0.38$ and $\Delta E_Q = 0.83$ mm/s. These parameters are essentially independent

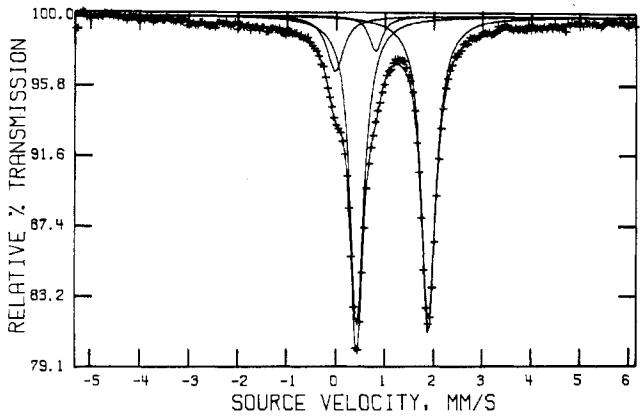

Figure 7. Room-temperature Mössbauer spectrum of $[Fe(DHBQ)(H_2O)_2]_n$. The solid curve is a fit to the parameters given in Table III[22] (9 mg of Fe/cm^2).

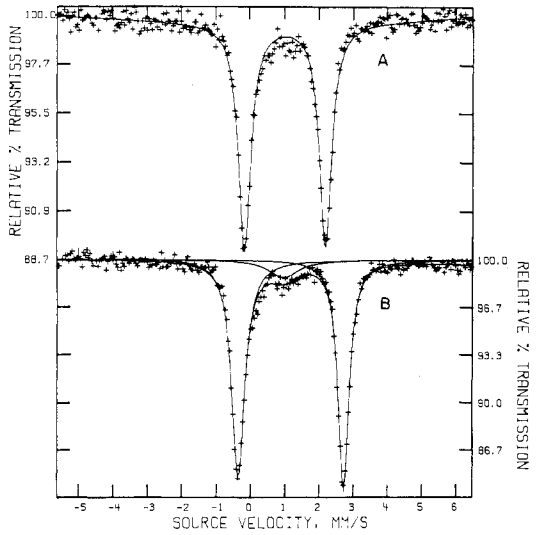

Figure 8. Mössbauer spectra of $[Fe(CA)(pyr)]_n$ (9 mg of Fe/cm^2): A = 295 K and B = 18 K. The solid curve in A is obtained for a single quadrupole doublet with parameters given in Table III.[22] Spectrum B contains an additional line at 1.0 mm/s.

of temperature in the range 300–15 K. We have *approximated* the relative fraction of Fe(III) in the sample by obtaining the ratio of the area of the Fe(III) doublet to the total area of the four Lorentzian lines (eq 4). The value of $f_{Fe^{3+}}$

$$f_{Fe^{3+}} = A_{Fe^{3+}}/(A_{Fe^{3+}} + A_{Fe^{2+}}) \quad (4)$$

obtained from four different preparations of $[Fe(DHBQ)(H_2O)_2]_n$ is 0.14 ± 0.04. This value was obtained from the room-temperature Mössbauer spectra. If the assumption is made that the Fe^{3+} sites are required for charge balance at terminal positions in the polymer, then an effective chain length of $11 < n < 20$ is obtained. We assume the Fe^{3+} is bound to the polymer because extensive washing of the polymer results in no change in its Mössbauer spectrum. We estimate that $f_{Fe^{3+}}$ for $[Fe(CA)(H_2O)_2]_n$ is <0.05. By using this value we obtain an effective chain length of $n > 40$ for $[Fe(CA)(H_2O)_2]_n$. These results are in qualitative agreement with the fits obtained for the magnetic susceptibility data for these compounds.

Mössbauer spectra of $[Fe(CA)(pyr)]_n$ at 295 K (spectrum A) and 18 K (spectrum B) are shown in Figure 8 and the parameters are given in Table III.[22] The high-temperature spectra obtained for $[Fe(DHBQ)(pyr)]_n$ are essentially superimposable on those for the CA analogue. At 295 K, a sharp quadrupole doublet with δ = 1.02 mm/s and ΔE_Q = 2.36 mm/s is observed for the CA complex. Upon cooling of the sample to 18 K, ΔE_Q and δ increase to 3.09 and 1.21 mm/s, respectively. The change in ΔE_Q is rather large to be explained by a second-order Doppler shift. It is unlikely that a phase transformation occurs in this temperature range because magnetic data do not substantiate this possibility.[42] We have found it necessary to include a third line of low intensity in the lower temperature data to adequately describe the spectra. This line is thought to be one line of an Fe(III) quadrupole doublet but our data do not warrant more detailed analysis of this effect.

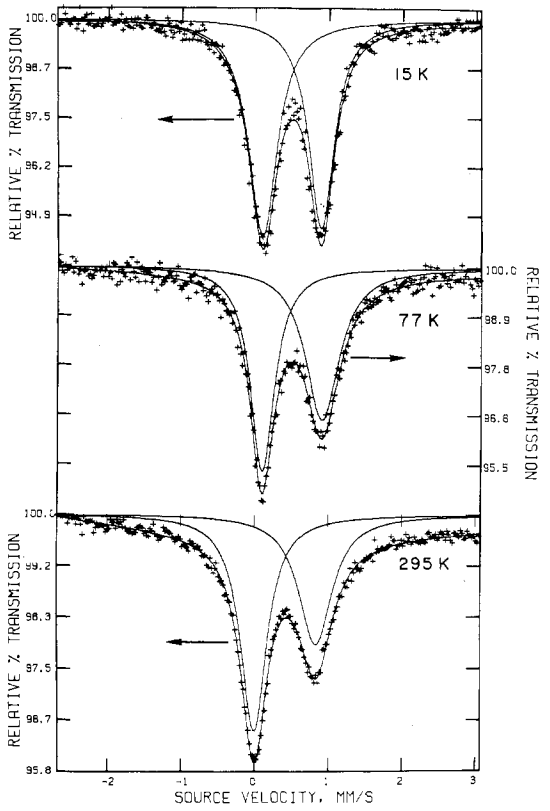

Figure 9. Mössbauer spectra of $Fe_2(DHBQ)_3(H_2O)_4$ taken at 295, 77, and 15 K (8 mg of Fe/cm^2). The solid curves represent fits to two lines with parameters given in Table III.[22]

Mössbauer Spectra of the Dimers. Mössbauer spectra of $Fe_2(DHBQ)_3(H_2O)_4$ taken at 295, 77, and 15 K are shown in Figure 9. The spectra of $Fe_2(CA)_3(H_2O)_4{\cdot}4H_2O$ at these temperatures are identical in form with those of the DHBQ dimer. Mössbauer spectral parameters for these two compounds are given in Table III.[22] The value of ΔE_Q for these dimers remains constant at approximately 0.80 mm/s in the temperature range 295–15 K. Both of these dimers show large line-intensity asymmetry at 295 K which decreases with decreasing temperature. In order to study in greater detail the nature of this asymmetry, we obtained Mössbauer spectra of the dimers at several temperatures. Results of the temperature behavior of the spectra are shown graphically in Figures 10 and 11, for $Fe_2(DHBQ)_3(H_2O)_4$ and $Fe_2(CA)_3(H_2O)_4{\cdot}4H_2O$, respectively.

Line-intensity asymmetry in Mössbauer hyperfine spectra may be a result of any one of the following factors or a combination of them: crystallite orientation, recoilless fraction anisotropy, and spin–spin or spin–lattice relaxation.[43] We have experimentally eliminated the problem of crystallite orientation by dispersing finely powdered samples in Vaseline for all of the spectra reported here. Relaxation effects are distinguished from the effect of Goldanskii–Karyagin (recoilless fraction) asymmetry by calculating the relative areas of the hyperfine quadrupole doublet lines. For line-intensity asymmetry due to relaxation effects the peak area ratio is unity whereas for

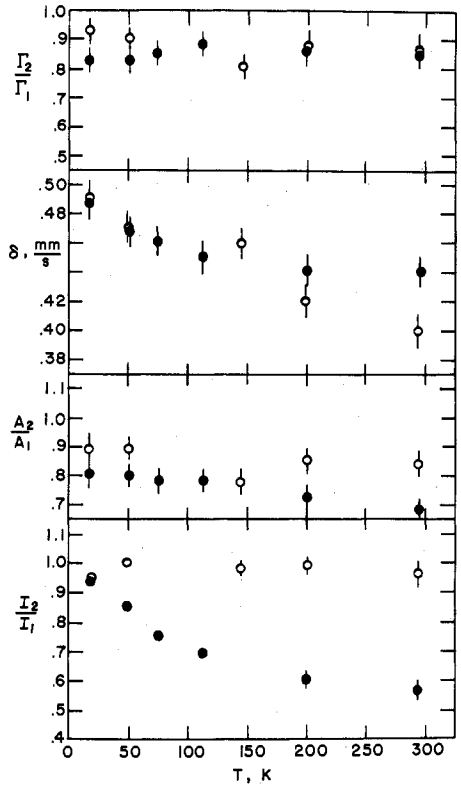

Figure 10. Plots of full-width at half maximum ratio (Γ_2/Γ_1), isomer shift (δ, mm/s), area ratio (A_2/A_1), and intensity ratio (I_2/I_1) vs. temperature for the quadrupole doublet of $Fe_2(DHBQ)_3(H_2O)_4$. Open circles (O) refer to data obtained for a "thick" absorber (~25 mg of Fe/cm^2). Full circles (●) refer to data obtained for a "thin" absorber (~8 mg of Fe/cm^2).

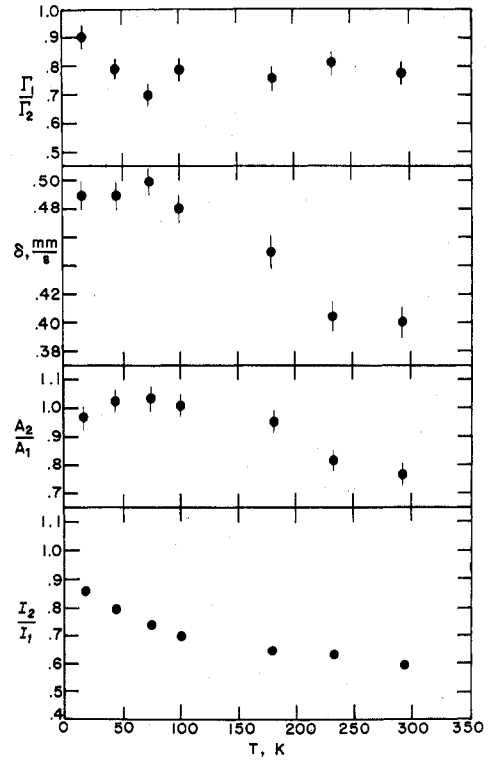

Figure 11. Plots of full-width at half maximum ratio (Γ_2/Γ_1), isomer shift (δ, mm/s), area ratio (A_2/A_1), and intensity ratio (I_2/I_1) vs. temperature for the quadrupole doublet of $Fe_2(CA)_3(H_2O)_4{\cdot}4H_2O$.

line-intensity asymmetry due to the Goldanskii–Karyagin effect the area ratio is different from unity.[44]

Table IV. Thermal Weight Loss Data[a]

compd	t,[b] °C	weight loss,[c] % obsd	weight loss,[c] % calcd
$Fe_2(CA)_3(H_2O)_4{\cdot}4H_2O$	100	9.4	8.2
	220	9.4	8.2
	~380	70.6	70.8
$Fe_2(DHBQ)_3(H_2O)_4$	240	12.0	12.1
	~370	70.0	69.3
$[Fe(CA)(H_2O)_2]_n$	250	11.6	12.1
$[Fe(DHBQ)(H_2O)_2]_n$	240	16.0	15.7
$[Fe(CA)(pyr)]_n$	300–400	80.6	83.7
$[Fe(DHBQ)(pyr)]_n$	300–400	80.2	79.6

[a] Obtained in air. [b] Temperature of inflection for the process. [c] % weight loss for the single process centered at that temperature.

On the basis of the data in Figures 10 and 11 we believe that the observed line-intensity asymmetry in $Fe_2(CA)_3(H_2O)_4{\cdot}4H_2O$ and $Fe_2(DHBQ)_3(H_2O)_4$ may be ascribed, at least to a first approximation, to the Goldanskii–Karyagin effect. We have thus far been unable to obtain single crystals of these dimers to check the orientation effect and thereby determine the sign of e^2qQ. However, integral asymmetry coupled with a nonunity area ratio does not support a large contribution to the asymmetry from relaxation effects.

Finally, we have investigated the effects on the relative line intensities for the dimers by obtaining Mössbauer spectra by using both thick and thin absorbers. Results of this study are also shown in Figure 10 for $Fe_2(DHBQ)_3(H_2O)_4$. Open circles in this figure represent data taken with a "thick" random absorber which contained approximately 25 mg of natural Fe/cm^2 while the full circles represent data taken with a "thin" absorber which contained 8 mg of Fe/cm^2. The difference between these two sets of data is significant only for the line-intensity ratio. Thus essentially no temperature dependence of I_2/I_1 is observed for the "thick" absorber whereas the asymmetry is very pronounced for the "thin" absorber. This observation may be qualitatively explained in terms of saturation effects[45] involving self-absorption in the absorber.

Thermal Analysis of the Complexes. Thermal weight loss data for the iron–dihydroxybenzoquinone complexes are given in Table IV. Processes which occur below 250 °C are well defined whereas those which occur at higher temperatures are very diffuse. These former processes are assigned to loss of water from the samples. Two low-temperature inflections are observed for $Fe_2(CA)_3(H_2O)_4{\cdot}4H_2O$. The first occurs at 100 °C and is assigned to loss of lattice water. The second occurs at 220 °C and, because it is identical with the 100 °C weight loss, is assigned to loss of coordinated water. Loss of coordinated water occurs at 240 °C for the DHBQ dimer. Both dimers showed broad weight loss profiles centered at approximately 375 °C. No organic matter was detected in the final residue which was shown by powder X-ray diffraction to be mainly Fe_2O_3. This final process is therefore due to gradual loss of the dihydroxybenzoquinone ligand. Both $[Fe(CA)(H_2O)_2]_n$ and $[Fe(DHBQ)(H_2O)_2]_n$ lose water near 240–250 °C. Only gradual decomposition of the material occurs in the range 280–550 °C. A complicated process occurs between 280 and 480 °C for the pyrazine-bridged polymers. Here again the final product is Fe_2O_3. The combined loss of pyrazine and dihydroxybenzoquinone ligands undoubtedly accounts for the complexity of the weight loss curve in this temperature range.

Infrared Spectra. $DHBQH_2$ and CAH_2 both display carbonyl stretching frequencies at approximately 1650 cm^{-1}. As expected, this absorption shifts to 1500 cm^{-1} in both of the dimers and aquo polymers. The carbonyl absorption shifts to 1540 cm^{-1} in $[Fe(CA)(pyr)]_n$ and $[Fe(DHBQ)(pyr)]_n$. The carbonyl band is much broader in the dimeric iron complexes than in the polymeric materials. This fact is consistent with

the presence of both bridging and terminal dihydroxybenzoquinone ligands in the dimers. In general the infrared spectra of the iron complexes of DHBQ and CA contain many fewer bands than the spectra of the parent ligands. Absence of these bands is entirely consistent with our formulation for these compounds. The pyrazine-containing polymers have infrared spectra which are consistent with the presence of bidentate pyrazine ligands. Thus, the ν(pyr) absorption at $\sim$1600 cm^{-1} is entirely absent in these compounds.[46]

Acknowledgment. The authors acknowledge financial support of this work by the Office of Naval Research.

Registry No. $[Fe(CA)(H_2O)_2]_n$, 67903-78-0; $[Fe(DHBQ)(H_2O)_2]_n$, 67903-82-6; $[Fe(CA)(pyr)]_n$, 68475-03-6; $[Fe(DHBQ)(pyr)]_n$, 67903-80-4; $Fe_2(CA)_3(H_2O)_4$, 68525-23-5; $Fe_2(DHBQ)_3(H_2O)_4$, 68540-15-8.

Supplementary Material Available: Listings of experimental and calculated magnetic susceptibilities and effective magnetic moments, Table I, and Mössbauer spectral parameters, Table III (7 pages). Ordering information is given on any current masthead page.

References and Notes

(1) R. S. Bottei and J. T. Fangman, *J. Inorg. Nucl. Chem.*, **28**, 1259 (1966).
(2) R. S. Bottei and D. L. Green, *J. Inorg. Nucl. Chem.*, **30**, 1469 (1968).
(3) A. M. Talati and V. N. Mistry, *Indian J. Chem.*, **11**, 296 (1973).
(4) D. K. Cabbiness and E. S. Amis, *Bull. Chem. Soc. Jpn.*, **40**, 435 (1967).
(5) A. M. Talati and V. N. Mistry, *J. Indian Chem. Soc.*, **50**, 225 (1973).
(6) H. Stone, A. B. Robertson, and M. T. Tetenbaum, U.S. Patent 3812066 (1973).
(7) S. Kanda and Y. Saito, *Bull. Chem. Soc. Jpn.*, **30**, 192 (1957).
(8) H. Kobayashi, T. Haseda, E. Kanda, and S. Kanda, *J. Phys. Soc. Jpn.*, **18**, 349 (1963).
(9) C. Yoshimura, H. Noguchi, T. Inoue, and H. Hara, *Bunseki Kagaku*, **15**, 918 (1966).
(10) N. A. A. Beg, *Pak. J. Sci. Ind. Res.*, **14**, 452 (1971).
(11) C. G. Pierpont, L. C. Francesconi, and D. N. Hendrickson, *Inorg. Chem.*, **16**, 2367 (1977).
(12) O. N. Kraschka, O. L. Atovmyan, and V. A. Avilov, *Tezisy Dokl.—Vses. Chugaevskoe Soveshch. Khim. Kompleksn. Soedin., 12th*, **2**, 244 (1975).
(13) D. K. Cabbiness, E. S. Amis, and K. C. Jackson, *J. Chem. Eng. Data*, **12**, 90 (1967).
(14) The design of this particular Faraday balance incorporates a Model CS-202 Displex cryogenic refrigerator manufactured by Air Products and Chemicals Inc., Allentown, Pa. This refrigerator operates on a helium cycle to achieve an ultimate temperature of 10 K. In order to eliminate vibration introduced by the Displex expander piston, an air-tight PVC membrane separated the electrobalance assembly from the expander. In this way noise levels due to Displex vibration were reduced to less than 10 μg.
(15) D. B. Brown, V. H. Crawford, J. W. Hall, and W. E. Hatfield, *J. Phys. Chem.*, **81**, 1303 (1977).
(16) F. E. Mabbs and D. J. Machin, "Magnetism and Transition Metal Complexes", Chapman and Hall, London, 1973, p 5.
(17) See, for example, S. N. Deming and S. L. Morgan, *Anal. Chem.*, **45**, 278A (1973), and references therein.
(18) Standard error = $\{\sum_{i=1}^{n}[\mu_{eff}(obsd)_i - \mu_{eff}(calcd)_i]^2/(n-k)\}^{1/2}$, where n is the number of data points and k is the number of fitting parameters: A. P. Ginsberg, R. L. Martin, R. W. Brookes, and R. C. Sherwood, *Inorg. Chem.*, **11**, 2884 (1972).
(19) C. W. Allen and D. B. Brown, *Inorg. Chem.*, **13**, 2020 (1974).
(20) J. T. Wrobleski, Doctoral Dissertation, University of Missouri—Rolla, 1977.
(21) R. B. Fischer and D. G. Peters, "Quantitative Chemical Analysis", W. B. Saunders, New York, N.Y., 1968, p 436.
(22) Supplementary material.
(23) B. N. Figgis, "Introduction to Ligand Fields", Interscience, New York, N.Y., 1966, p 280.
(24) J. T. Wrobleski and D. B. Brown, unpublished results.
(25) J. T. Wrobleski and D. B. Brown, *Inorg. Chem.*, **17**, 2959 (1978).
(26) J. A. Thich, C. C. Ou, D. Powers, B. Vasiliou, D. Mastropaolo, J. A. Potenza, and H. J. Schugar, *J. Am. Chem. Soc.*, **98**, 1425 (1976).
(27) W. M. Reiff, W. A. Baker, Jr., and N. E. Erickson, *J. Am. Chem. Soc.*, **90**, 4794 (1968).
(28) A. V. Khedekar, J. Lewis, F. E. Mabbs, and H. Weigold, *J. Chem. Soc.*, 1561 (1967).
(29) T. R. Felthouse, E. J. Laskowski, and D. N. Hendrickson, *Inorg. Chem.*, **16**, 1077 (1977).
(30) B. N. Figgis, J. Lewis, F. E. Mabbs, and G. A. Webb, *J. Chem. Soc. A*, 442 (1967).
(31) Reference 16, p 131.
(32) See, for example: J. N. McElearney, *Inorg. Chem.*, **15**, 823 (1976); R. Dingle, M. E. Lines, and S. L. Holt, *Phys. Rev.*, **187**, 643 (1969); J. N. McElearney, *Inorg. Chem.*, **17**, 248 (1978).
(33) S. Katsura, *Phys. Rev.*, **127**, 1508 (1962); M. E. Fisher, *J. Math. Phys. (N.Y.)*, **4**, 124 (1963).
(34) Certain inadequacies in the Ising model for the present purpose are well documented. See, for example: R. W. Jotham, *J. Chem. Soc., Chem. Commun.*, 178 (1973).
(35) M. Habenschuss and B. C. Gerstein, *J. Chem. Phys.*, **61**, 852 (1974).
(36) A. Santoro, A. D. Mighell, and C. W. Reimann, *Acta Crystallogr., Sect. B*, **26**, 979 (1970).
(37) S. A. Adeyemi, E. C. Johnson, F. J. Miller, and T. J. Meyer, *Inorg. Chem.*, **12**, 2371 (1973).
(38) P. W. Carreck, M. Goldstein, E. M. McPartlin, and W. D. Unsworth, *Chem. Commun.*, 1634 (1971).
(39) D. B. Losee, H. W. Richardson, and W. E. Hatfield, *J. Chem. Phys.*, **59**, 3600 (1973).
(40) Unless otherwise stated, Mössbauer parameters presented herein have the following maximum uncertainties: δ, $\pm$0.03 mm/s; ΔE_Q, $\pm$0.03 mm/s; Γ_2/Γ_1, $\pm$0.08; A_2/A_1, $\pm$0.08; I_2/I_1, $\pm$0.04.
(41) R. V. Pound and G. A. Rebka, Jr., *Phys. Rev. Lett.*, **4**, 274 (1960); B. D. Josephson, *ibid.*, **4**, 341 (1960).
(42) We thank a reviewer for pointing out that the large change in ΔE_Q may result from a change of the Boltzman population of the t_{2g} set of orbitals with a change in temperature and resulting in a change in the **EFG** tensor.
(43) See, for example: N. N. Greenwood and T. C. Gibb, "Mössbauer Spectroscopy", Chapman and Hall, London, 1971, pp 66–77.
(44) V. I. Goldanskii and E. F. Makarov, "Chemical Applications of Mössbauer Spectroscopy", V. I. Goldanskii and R. H. Herber, Ed., Academic Press, New York, N.Y., 1968, pp 102–107.
(45) T. C. Gibb, R. Greatrex, and N. N. Greenwood, *J. Chem. Soc. A*, 890 (1968).
(46) The symmetric pyrazine stretch near 1600 cm^{-1} is IR inactive for bidentate pyrazine: M. Goldstein and W. D. Unsworth, *Spectrochim. Acta, Part A*, **27a**, 1055 (1971).